New Phytologist

Research

MLO-mediated Ca^{2+} influx regulates root hair tip growth in Arabidopsis

Sienna T. Ogawa[1,2], Weiwei Zhang[1,2,3], Christopher J. Staiger[1,2,3] and Sharon A. Kessler[1,2]

[1]Department of Botany and Plant Pathology, Purdue University, 915 Mitch Daniels Blvd, West Lafayette, IN 47907, USA; [2]Purdue Center for Plant Biology, Purdue University, 915 Mitch Daniels Blvd, West Lafayette, IN 47907, USA; [3]EMBRIO Institute, Purdue University, 207 S. Martin Jischke Ave, West Lafayette, IN 47907, USA

Author for correspondence:
Sharon A. Kessler
Email: kessles@purdue.edu

Received: *28 January 2025*
Accepted: *13 June 2025*

New Phytologist (2025)
doi: 10.1111/nph.70378

Key words: calcium, FERONIA, MLO, root hair, ROS, tip growth.

Summary

- Root hair tip-growth involves coordinated Ca^{2+} and ROS signaling to promote growth while maintaining tip integrity. MILDEW RESISTANCE LOCUS-O (MLO) proteins act downstream of FERONIA (FER) receptor-like kinases in pollen tubes and synergids to regulate calcium dynamics. This study uses a constitutively active MLO (faNTA) to identify a new role for the FER/MLO signaling module in regulating $[Ca^{2+}]_{cyt}$ oscillations in growing root hairs.
- faNTA was used as a tool to manipulate Ca^{2+} influx in *fer* mutants. Light sheet fluorescence imaging was used to image the reporter R-GECO1 to observe $[Ca^{2+}]_{cyt}$ dynamics during root hair elongation in various genotypes.
- We show that faNTA is sufficient to restore normal root hair development, $[Ca^{2+}]_{cyt}$ oscillations, and ROS levels to *fer-4*. MLO15 was identified as a regulator of root hair tip growth based on disrupted root hair growth and $[Ca^{2+}]_{cyt}$ signatures in *mlo15-4*. We also link the FER/MLO module to ROS accumulation by showing that faNTA is sufficient to restore ROS levels in *fer-4* root hairs, but is unable to complement the burst root hairs of *rbohc*.
- We propose that MLOs act downstream of FER to mediate Ca^{2+} influx and promote ROS production to regulate root hair tip growth.

Introduction

Plant cells respond to and explore their environments by regulating growth. For example, root hairs are initiated from bulges in epidermal cells and extend out into the soil to maximize water and nutrient absorption. In these tip-growing cells, the site of cell expansion is confined to the apical tip, resulting in long cells with a uniform width. This tip growth is modulated through the coordination of a number of factors, including polarized secretion, cytoskeletal networks, and cell wall modifications (Cole & Fowler, 2006; Mendrinna & Persson, 2015; Takatsuka & Ito, 2020). Furthermore, tip-focused gradients of protons (H^+), reactive oxygen species (ROS), and cytoplasmic calcium ($[Ca^{2+}]_{cyt}$) are associated with polarized growth (Monshausen *et al.*, 2008; Stéger & Palmgren, 2022; Lopez *et al.*, 2024). In Arabidopsis root hairs, H^+ oscillations mediated by AHA2 and AHA7 occur at the root hair apex (Monshausen *et al.*, 2007; Hoffmann *et al.*, 2019). The tip-focused ROS gradient in root hairs is generated by the NADPH oxidase encoded by RESPIRATORY BURST HOMOLOG C/ROOT HAIR DEFECTIVE 2 (RBOHC/RHD2) (Foreman *et al.*, 2003; Monshausen *et al.*, 2007). Root hairs also display a tip-focused $[Ca^{2+}]_{cyt}$ gradient. $[Ca^{2+}]_{cyt}$ oscillations are correlated with root hair elongation (Bibikova *et al.*, 1997; Monshausen *et al.*, 2008). In root hairs, crosstalk between pH, ROS, and Ca^{2+} has been observed, but how this crosstalk is regulated remains poorly understood (Monshausen *et al.*, 2009).

One way ROS/Ca^{2+} crosstalk occurs is through ROS-mediated activation of hyperpolarized-activated calcium channels (HACCs) expressed at the root tip to mediate the tip-focused $[Ca^{2+}]_{cyt}$ gradient and oscillations during tip growth. The presence of HACCs at the root tip was supported by electrophysiology studies, but until recently, the identity of these channels remained unknown (Véry & Davies, 2000). Four members of the CYCLIC NUCLEOTIDE GATED CHANNEL family (CNGC 5, 6, 9, 14) mediate Ca^{2+} influx in root hairs. Seedlings of the *cngc14* mutant develop short and branched root hairs when roots are grown in media, but appear normal when grown on the surface of vertical plates, indicating that these root hairs are compromised in their ability to respond to the external environment (Zhang *et al.*, 2017). When multiple root hair-expressed CNGC genes are knocked out, root hairs are shorter, branched, and frequently burst, indicating problems with maintaining polarized tip growth (Brost *et al.*, 2019; Tan *et al.*, 2020; Zhu *et al.*, 2025). These mutant root hairs have altered $[Ca^{2+}]_{cyt}$ oscillations that occur at a lower amplitude and frequency than in the wild-type root hairs (Brost *et al.*, 2019). Receptor-like kinases are good candidates for regulating Ca^{2+} channels in response to external signals. The *Catharanthus roseus* receptor-like kinase (CrRLK1L) $[Ca^{2+}]_{cyt}$-ASSOCIATED PROTEIN KINASE 1 (CAP1)/ERULUS (ERU) functions as a regulator of Ca^{2+} influx in root hairs (Kwon *et al.*, 2018). The root hairs of *eru* mutants are short and have altered $[Ca^{2+}]_{cyt}$ oscillations that occur less frequently, but

at higher amplitudes than the wild-type (Kwon *et al.*, 2018). The Ca^{2+} channels regulated by ERULUS are unknown, and it remains unclear whether other families of Ca^{2+} channels contribute to tip growth in root hairs.

In other cell types throughout the plant, CrRLK1Ls function as regulators of MILDEW RESISTANCE LOCUS-O (MLO) proteins (Ju *et al.*, 2021; Gao *et al.*, 2022, 2023). The first MLO gene was identified as a powdery mildew susceptibility factor in barley (Büschges *et al.*, 1997). Since then, members of the MLO family have been implicated in roles throughout the plant, including root tropism, pollen tube growth, and pollen tube reception (Chen *et al.*, 2009; Kessler *et al.*, 2010; Bidzinski *et al.*, 2014; Meng *et al.*, 2020; Gao *et al.*, 2022, 2023). Recently, MLO genes in Arabidopsis were characterized as Ca^{2+} influx channels (Gao *et al.*, 2022). NORTIA (NTA, MLO7) regulates the amplitude of $[Ca^{2+}]_{cyt}$ oscillations in synergids during pollen tube reception (Ngo *et al.*, 2014). The CrRLK1L protein FERONIA (FER) is necessary for the initiation of $[Ca^{2+}]_{cyt}$ oscillations upon pollen tube arrival at the female gametophyte (Ngo *et al.*, 2014). NTA acts downstream of FER: NTA is Golgi-retained before pollination and accumulates in a membrane-rich region known as the filiform apparatus in a FER-dependent manner as the pollen tube approaches (Ju *et al.*, 2021). Our lab discovered that a chimeric protein generated by swapping the C-terminus of NTA with the MLO1 C-terminus (faNTA) accumulates constitutively at the filiform apparatus both before and after pollination (Ju *et al.*, 2021). faNTA can bypass FER signaling in synergids and is sufficient to suppress infertility in *fer-1* (Ju *et al.*, 2021). These data suggest that faNTA functions as a constitutively activated MLO because it can mediate Ca^{2+} influx at the filiform apparatus independent of FER signaling. In support of this, faNTA accumulates at the plasma membrane in mammalian HEK293 cells and is able to mediate Ca^{2+} influx, while NTA is not plasma membrane localized and instead accumulates in cytoplasmic puncta and is unable to mediate Ca^{2+} influx (Gao *et al.*, 2022).

While NTA is only expressed in synergids, FER is expressed widely throughout the plant and has been implicated in a variety of cellular processes (Ogawa & Kessler, 2023; Cheung, 2024). The *fer* mutants exhibit multiple pleiotropic phenotypes, ranging from infertility due to a failure of pollen tubes to burst during pollen tube reception to root hairs that burst instead of maintaining tip growth (Escobar-Restrepo *et al.*, 2007; Duan *et al.*, 2010). The root hair bursting that occurs in *fer* has been attributed to reduced ROS levels due to a failure in FER-mediated ROP-GEF regulation of RBOHC (Duan *et al.*, 2010). Since the regulation of root hair tip growth and maintenance of tip integrity has also been linked to the maintenance of $[Ca^{2+}]_{cyt}$ oscillations, we hypothesized that FER might also regulate $[Ca^{2+}]_{cyt}$ oscillations in growing root hairs through regulation of Ca^{2+} channels. In this study, we test this hypothesis by expressing the constitutively active MLO channel, faNTA, broadly in *fer* mutants and show that it restores tip integrity to *fer* root hairs. We also show that *fer-4* mutants have abnormal $[Ca^{2+}]_{cyt}$ oscillations that occur with erratic amplitudes and altered frequency that can be restored to wild-type patterns by expressing faNTA. Furthermore, faNTA is sufficient to restore tip integrity and normal root hair elongation to *fer* mutants, while also restoring ROS to wild-type levels. Finally, we show that MLO15 is expressed in growing root hairs and contributes to root hair elongation by regulating $[Ca^{2+}]_{cyt}$ oscillations at the root hair tip. Our study defines a new role for MLO proteins as regulators of $[Ca^{2+}]_{cyt}$ oscillations during root hair elongation.

Materials and Methods

Plant materials and growth conditions

Arabidopsis thaliana (L.) ecotypes Col-0 and Ler were used as wild-type controls. Seeds were surface-sterilized and plated on ½-strength Murashige and Skoog (MS) medium with 1% sucrose with or without selection. For transgenic selection, the plates were supplemented with hygromycin to a final concentration of 20 mg l^{-1}. Seeds were stratified at 4°C for 2 d before being transferred to a growth chamber (22°C, 16 h : 8 h, light : dark cycle). The *fer-1* mutant was generously provided by Prof. Ueli Grossniklaus (Escobar-Restrepo *et al.*, 2007). Insertion lines for *mlo15-4* (CS66561), *fer-4* (CS69044), and *rhd2-1* (CS2259) were obtained from the Arabidopsis Biological Resource Center (ABRC). The *Arabidopsis thaliana* R-GECO1 reporter line (Keinath *et al.*, 2015) was kindly provided by Melanie Krebs (University of Heidelberg).

Cloning and generation of transgenic lines

PCR amplification with Q5 High-Fidelity DNA Polymerase was used to generate the following constructs with Gateway cloning. Entry vector pDONR207-faNTA was described previously (Ju *et al.*, 2021). pDONR207-faNTA was recombined via LR reaction into p184 (Myers *et al.*, 2016) and pMDC83 (Curtis & Grossniklaus, 2003) with pFER promoter to generate 35S::faNTA-YFP and pFER::faNTA-GFP, respectively. MLO15 was amplified from gDNA with primers MLO15F (GGGGACAAGTTTGTACAAAAAAGCAGGCTTCACCATGGCGGGAGGAG) and MLO15R (GGGGACCACTTTGTACAAGAAAGCTGGGTGATCATGGTGAGCAATCTCT). The MLO15 entry vector was generated via BP reaction with pDONR207 as the backbone. pDONR207-MLO15 was recombined via LR reaction into pMDC83 to generate 35S::MLO15-GFP. pMLO15::MLO15-GFP was previously described (Davis *et al.*, 2017). For complementation assays, expression vectors were introduced into *Agrobacterium tumefaciens* GV3101 and transformed into *mlo15-4*, *fer-4, fer-1*/+, and *rhd2-1* using the floral-dip method (Clough & Bent, 1998). Transgenic lines were screened on hygromycin or Basta, and homozygous T3 or T4 lines were used for experiments.

Root hair phenotyping, quantification, and live imaging

Five-day-old vertically grown seedlings were mounted in water and imaged with a Nikon Ti2 microscope. A region of the primary root, 2–3 mm above the root tip, was chosen for

phenotyping because this is the area where *fer* root hair phenotypes are visible and root hairs have not yet burst completely. For *35S::faNTA-YFP; rhd2-1* lines, T1 seeds were grown under Basta selection for 5 d, then transferred to selection-free plates for 2 d before roots were imaged and root hair lengths quantified 2–3 mm from the primary root tip. For these lines, YFP intensity was observed on a Nikon Eclipse Ti-2 epifluorescence microscope with a 20× objective to confirm faNTA expression. Root hairs were categorized as tip-growing if they were intact and had polarized growth, burst, or spherical if there was no polarity. Tip-growing root hairs were used for tip width/base width analysis. The tip width was measured 10 µm from the root hair tip, and the base width was measured at the root hair base. The tip width/base width ratio was determined for all tip-growing root hairs, and lines were compared with a one-way ANOVA with Tukey test in GraphPad Prism 10.

To quantify root hair length along the entirety of the primary root, 7-d-old vertically grown seedlings were mounted in water and imaged with a Nikon Ti2 microscope. Root hair length and the distance of that root hair from the root tip were measured using ImageJ (Schindelin *et al.*, 2012).

For timelapse imaging of root hairs, seeds were plated on ½ MS with 1% sucrose and stratified for 2 d at 4°C. Plates were then grown vertically in a growth chamber for 5 d. Seedlings were transferred to slides and mounted in liquid 1/10-strength MS medium without sucrose. Parafilm was used to secure the cover slip to the slide, and slides were placed vertically in a box with 1/10 MS. The slides were returned to the growth chamber overnight so the seedlings could acclimate. Root hairs that were closest to the root tip were imaged every 5 min for 2 h on a Nikon Ti-2 microscope in a room maintained at 21–22°C. Root hair length was measured at each time point in ImageJ, and the increase in length was plotted over time in Graphpad Prism 10 to obtain the average growth rate as the slope of the linear regression.

Light sheet fluorescence microscopy sample preparation

Seeds were surface sterilized and stratified on ½ MS 1% sucrose plates for at least 2 d. Glass capillary tubes (100 µl; BR708744; Sigma-Aldrich) were cut to the length of the sample holder. Ethylene propylene (FEP) tubing (Bruker Nano Inc., Berlin, Germany) with an inner diameter of 1.7 mm was pre-cleaned by washing with 1 M NaOH and 70% EtOH as previously described (Weber *et al.*, 2014). FEP tubing was cut to a 50 mm length and inserted onto the glass micropipette tubes and autoclaved. To prepare samples, the capillary tube/FEP tube was filled with ½ MS, 1% sucrose, 0.5% phytagel medium, and a stratified seed was placed on the media at the top of the FEP tube. To keep samples humid and upright, 1 ml pipette tips were cut and inserted into sterile jars with 1% agar with a thin layer of water over the top. The capillary/FEP tube with the seed was then inserted into the 1 ml pipette tip vertically, and the jar was covered with a Petri dish secured with micropore tape. This system was moved into a growth chamber, and seeds were allowed to grow for 5 d until root tips were at the bottom of the FEP tubing, but not yet growing through the glass capillary tube.

Subcellular localization of MLO15

The complemented line *pMLO15::MLO15-GFP;mlo15-4* was imaged on a Bruker MuVi SPIM light sheet microscope equipped with two Nikon CFI Plan Fluor 10× W 0.3 NA water immersion objective lenses for illumination and two Olympus XLUMPLFLN 20× (eff. 22.2×) W 1.0 NA water immersion objective lenses for detection. The capillary tube/FEP tube with a 5-d-old growing seedling was inserted vertically into the imaging chamber filled with water, keeping the cotyledons out of the water for the duration of imaging. A 2.5 µm beam expander was used. Images were acquired with 10% 488 nm laser intensity, BP 500-530 filter, 50 ms exposure, and a 3 µm step size (175 steps total) every 5 min for 4 h. Images were collected using single side illumination with a Hamamatsu ORCA-Fusion BT CMOS camera. Maximum intensity projections were generated for each time frame in ImageJ.

For laser scanning confocal microscopy, seedlings were incubated in 20 µM FM4-64 (T3166; Molecular Probes, Eugene, OR, USA) in PIPES Buffer (50 mM PIPES, 5 mM EGTA, and 1 mM $MgSO_4$ at pH 6.8) for 5 min before imaging. Imaging was performed on a Zeiss LSM 880 upright confocal microscope with a 10× objective and 10% laser intensity. Seedlings were imaged with a 488 nm excitation wavelength, and emission was captured between 485–560 nm for GFP/YFP and 600–850 nm for FM4-64. Image analysis was done in ImageJ. Fluorescence intensity profiles for GFP and FM4-64 intensity were generated in ImageJ using the Plot Profile function along three parallel lines through the root hair. Average intensity was plotted over distance with error bars representing the SD.

R-GECO1-based live Ca^{2+} imaging in root hairs

The intensiometric cytosolic Ca^{2+} sensor R-GECO1 (Keinath *et al.*, 2015) was crossed from Col-0 into *35S::MLO15* and *mlo15-4*. Homozygous F3 seedlings were grown in FEP tubing as described above and imaged on a Bruker MuVi SPIM light sheet microscope with the same objectives and set up as described above. Images were acquired with a 10% 561 nm laser and a 580-627 BP filter with a line scan width of 50 pixels. A 50-ms exposure and 5 µm step size (for 3 steps) were used to image root hairs every 3 s for 12 min. The last 10 min of the image acquisition was used for further analysis to control for signal alterations at the start due to laser illumination.

Sum intensity projections were generated in ImageJ and used for analysis. Images were cropped to only contain a single root hair and were converted from 16-bit to 8-bit. The TrackMate plugin in ImageJ was used to track the brightest signal in the root hair apex, and the mean fluorescence intensity was obtained for each frame (Tinevez *et al.*, 2017). The brightest signal was detected as a 30-pixel diameter region of interest (ROI) with the LoG detector in TrackMate and tracked in each frame. The mean fluorescence intensity was obtained from the ROI for each frame for calcium oscillation analysis. The background signal was subtracted for each frame individually. Intensity traces were normalized as $\Delta F/F_0$. We used the background-subtracted R-GECO1

intensity in a 400 pixel^2 window in the shank of the root hair as F_0. Peak intensity extraction was performed in MATLAB with the *findpeaks* function. Fourier transform and power spectral density (PSD) analysis were performed in MATLAB as previously described (Candeo *et al.*, 2017). The relevant MATLAB code can be found in the link: https://github.com/SADDLab/Root_Hair_Calcium_Analysis_Toolkit.git.

H2DCF-DA and Peroxy Orange 1 reactive oxygen species (ROS) staining in root hairs

Five-day-old vertically grown seedlings were stained using the protocol described in Gayomba & Muday (2020). For H2DCF-DA staining, seedlings were incubated in 25 μm CM-H2DCFDA (C6827; Thermo Fisher) made from a 50-mM stock in DMSO and diluted in water for 4 min. Seedlings were mounted in water and imaged with a Zeiss LSM 880 upright confocal microscope with a 10× objective, 5% laser intensity, and 1 airy unit pinhole with GFP optics. For PO1 staining, seedlings were incubated in 50 μm PO1 (4944; R&D Systems, Minneapolis, MN, USA) for 15 min in the dark. Seedlings were rinsed and mounted in water. Images were acquired with a 488 nm laser and 544–695 emission filter using 5% laser intensity and a pinhole size of 1 airy unit. For both stains, images of primary roots containing initiating and early growth stage root hairs were analyzed as 8-bit maximum intensity projections. For each root hair, the mean fluorescence intensity was taken along a line from base to tip in IMAGEJ (Schindelin *et al.*, 2012). Statistical comparison was done using a one-way ANOVA with a Tukey test in GRAPHPAD PRISM 10.

Results

faNTA is sufficient to complement *fer-4* root hair development

$[Ca^{2+}]_{cyt}$ oscillations that occur at consistent amplitude and frequency at the root hair tip are correlated with maintenance of root hair polarity and growth, but it is not clear if FER regulates the amplitude or frequency of these $[Ca^{2+}]_{cyt}$ oscillations during root hair tip growth. Since faNTA is sufficient to bypass FER signaling in synergids and induce pollen tube bursting in *fer-1*, we hypothesized that increasing $[Ca^{2+}]_{cyt}$ in root hairs through faNTA expression would also suppress the burst root hair phenotype of *fer* by bypassing FER signaling. To test this hypothesis, faNTA was expressed in *fer* mutants under the control of the constitutive Cauliflower Mosaic Virus 35S promoter (Odell *et al.*, 1985) and the FER promoter to ensure that faNTA would be expressed in the same tissues as FER. Laser scanning confocal microscopy (LSCM) revealed that faNTA-YFP is present at the plasma membrane in initiating, elongating, and mature root hairs (Supporting Information Fig. S1a).

To test for complementation of the *fer* phenotype, early elongating root hairs on the primary root were measured in Col-0, *fer-4*, and *35S::faNTA;fer-4* (Fig. 1a). Compared to wild-type root hairs that had an average length of 272 ± 61 μm, *fer-4* root hairs were significantly shorter with an average length of 83 ± 40 μm. The reduced root hair length of *fer-4* was restored to 266 ± 59 μm in *35S::faNTA;fer-4*, which is not significantly different from Col-0 (Fig. 1b). The same complementation of root hair length was observed when *35S::faNTA* and *pFER::faNTA* were expressed in the *fer-1* allele in the Landsberg *erecta* (Ler) background (Fig. S1b,c), indicating that promoter strength and genetic background did not play a role in the ability of faNTA to complement the *fer* root hair phenotype.

In addition to the previously reported *fer* root hair bursting phenotype seen in 33% of root hairs, we observed two phenotypes that have not been previously described. The majority of *fer* root hairs in the early elongation zone were anisotropic and tip-growing but were cone-shaped with thicker bases than tips compared to wild-type root hairs. The remaining 25% of the root hairs were spherical and lacked polarized tip growth (Fig. 1a,c,d). Spherical root hairs were never observed in Col-0 or *35S::faNTA;fer-4* root hairs. To determine whether *35S::faNTA* complements the altered tip-growing root hair shape in *fer-4*, the tip width/base width ratio was calculated. Col-0 has a tip/base ratio of 0.89 ± 0.20 and *fer-4* has a ratio of 0.55 ± 0.021 (Fig. 1d). *35S::faNTA;fer-4* root hairs have a tip/base ratio of 0.85 ± 0.18, indicating that expression of faNTA is sufficient to complement root hair shape in a *fer-4* background (Fig. 1d). The tip growing and spherical root hairs in *fer-4* are only found shortly after initiation and then eventually burst, which is likely why they have not been previously described.

fer root hairs have altered Ca^{2+} oscillations that are complemented with faNTA

The loss of tip integrity in *fer-4* root hairs has been attributed to a reduction in ROS, but Ca^{2+} dynamics have not been explored in *fer-4* root hairs (Duan *et al.*, 2010). We predicted that expression of faNTA in *fer-4* might lead to a larger influx of Ca^{2+} during oscillations that could contribute to root hair elongation and tip maintenance. To observe Ca^{2+} oscillations in wild-type, *fer-4*, and *35S::faNTA-YFP;fer-4* root hairs, the intensiometric cytoplasmic Ca^{2+} sensor R-GECO1 (Keinath *et al.*, 2015) was crossed into these lines. To confirm that all lines in our study expressed R-GECO1 at similar levels and would therefore have a similar response to extracellular ATP, exogenous ATP was added to roots and R-GECO1 intensities were measured (Demidchik *et al.*, 2003). The maximum normalized fluorescence value in the primary root elongation zone after ATP treatment confirmed that all of the genotypes used in our study expressed similar levels of R-GECO1 (Fig. S2a–d,g; Methods S1).

Our analysis of faNTA complementation of *fer* phenotypes was performed on seedlings grown on the surface of vertical plates containing plant growth media (Fig. 1). Light sheet fluorescence microscopy (LSFM) allows seedlings to grow vertically in tubes that are then imaged vertically, reducing the amount of sample handling and more closely mimicking natural growing conditions. Light sheet fluorescence microscopy was used to image early elongating root hairs every 3 s for 10 min, and R-GECO1 intensity at the root tip was measured, similar to the LSFM imaging and analysis done with Yellow Cameleon 3.6

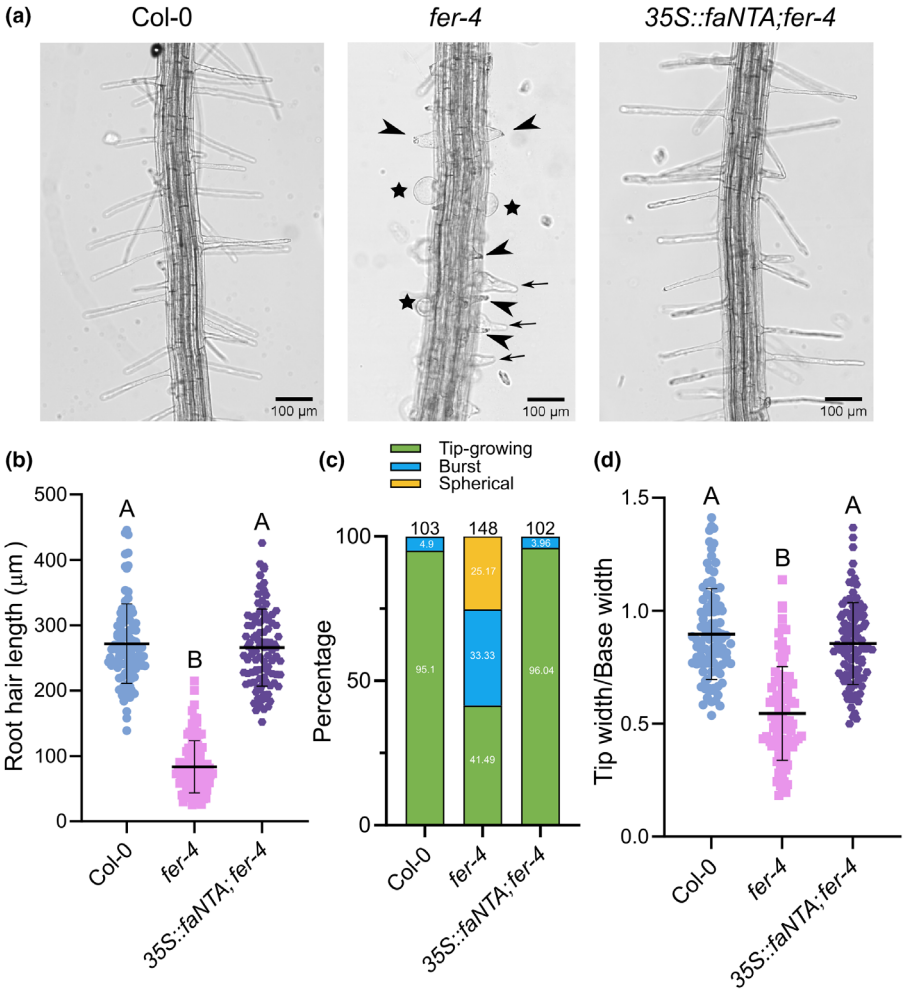

Fig. 1 faNTA complements the abnormal root hair development of Arabidopsis *fer-4*. (a) Col-0, *fer-4*, and *35S::faNTA;fer-4* root hairs were imaged and phenotyped in a 1-mm region that was located 2–3 mm from the primary root tip. For *fer-4*, stars indicate spherical root hairs, arrows indicate tip-growing root hairs, and arrowheads indicate burst root hairs. Bars, 100 µm. (b) The length of early elongating root hairs was measured for Col-0 (n = 99), *fer-4* (n = 101), and *35S::faNTA;fer-4* (n = 99). (c) The percentage of Col-0 (n = 103), *fer-4* (n = 148), and *35S::faNTA;fer-4* (n = 102) root hairs that are tip-growing, burst, or spherical. (d) The width of root hair tip divided by the width of root hair base was calculated for individual root hairs for Col-0 (n = 100), *fer-4* (n = 95), and *35S::faNTA;fer-4* (n = 100). The *fer-4* root hairs have wider root hair bases than tips. Multiple comparison analysis was done in GraphPad Prism 10 as a one-way ANOVA with a Tukey test, $P < 0.05$. Different letters indicate a significant difference, and horizontal lines in plots indicate mean ± SD.

(Candeo *et al.*, 2017). For image analysis, R-GECO1 intensity at the root hair apex was normalized to R-GECO1 intensity in the shank to exclude possible R-GECO1 expression differences between seedlings or individual root hairs. Normalized intensity traces show that tip-growing *fer-4* root hairs have erratic oscillations that do not occur at regular intervals and display a larger variation in amplitude than Col-0 root hairs that oscillate with consistent frequency and amplitude over the imaging period (Fig. 2a, additional traces S3, Videos S1, S2). In contrast to the tip-growing *fer-4* root hairs, spherical *fer-4* root hair $[Ca^{2+}]_{cyt}$ oscillations occurred at very low amplitude and frequency so only tip-growing root hairs were used for further analysis. Normalized intensity traces of *35S::faNTA;fer-4* root hairs show that 35S::faNTA restores normal oscillation timing and amplitude to *fer-4* (Fig. 2a, additional traces S3, Video S2).

To quantify the differences in $[Ca^{2+}]_{cyt}$ oscillation amplitude between Col-0, tip growing *fer-4*, and *35S::faNTA;fer-4* root hairs, the normalized intensity value for each oscillation peak was extracted for individual root hairs. The average normalized peak intensity is not different between lines (Fig. 2b), likely because *fer-4* oscillations occur at amplitudes both higher and lower than Col-0. The SD between normalized peak intensities was calculated for individual root hairs and plotted to better represent the range of amplitudes in *fer-4* tip growing root hairs (Fig. 2c). The average SD in peak intensity is higher in *fer-4* than in the wild-type, and the average SD for *35S::faNTA;fer-4* is not significantly different from both Col-0 and *fer-4* (Fig. 2c). Within *fer-4*, SD varies with some root hairs having similar values as Col-0, with some root hairs having much higher SD (Fig. 2c). These data, along with the normalized intensity traces, show that *fer-4* tip-growing root hairs have erratic $[Ca^{2+}]_{cyt}$ oscillations with altered amplitude.

fer-4 root hairs appear to have fewer $[Ca^{2+}]_{cyt}$ oscillations than Col-0 in the normalized intensity traces (Figs 2a, S3). To quantify changes in $[Ca^{2+}]_{cyt}$ oscillation frequency, normalized R-GECO1 intensity data were Fourier transformed and the PSD calculated as described in Candeo *et al.* (2017) to determine the interval of $[Ca^{2+}]_{cyt}$ oscillations in Col-0, *fer-4*, and *35S::faNTA;fer-4* root hairs. Col-0 root hairs have a single peak at 0.038 Hz, which corresponds to oscillations occurring every 26.3 s (Fig. 2d). This result is consistent with the 0.036 Hz frequency reported for Col-0 root hairs expressing the ratiometric $[Ca^{2+}]_{cyt}$ reporter Yellow Cameleon 3.6 (YC3.6) imaged with light sheet microscopy, and the 0.036–0.038 Hz frequency

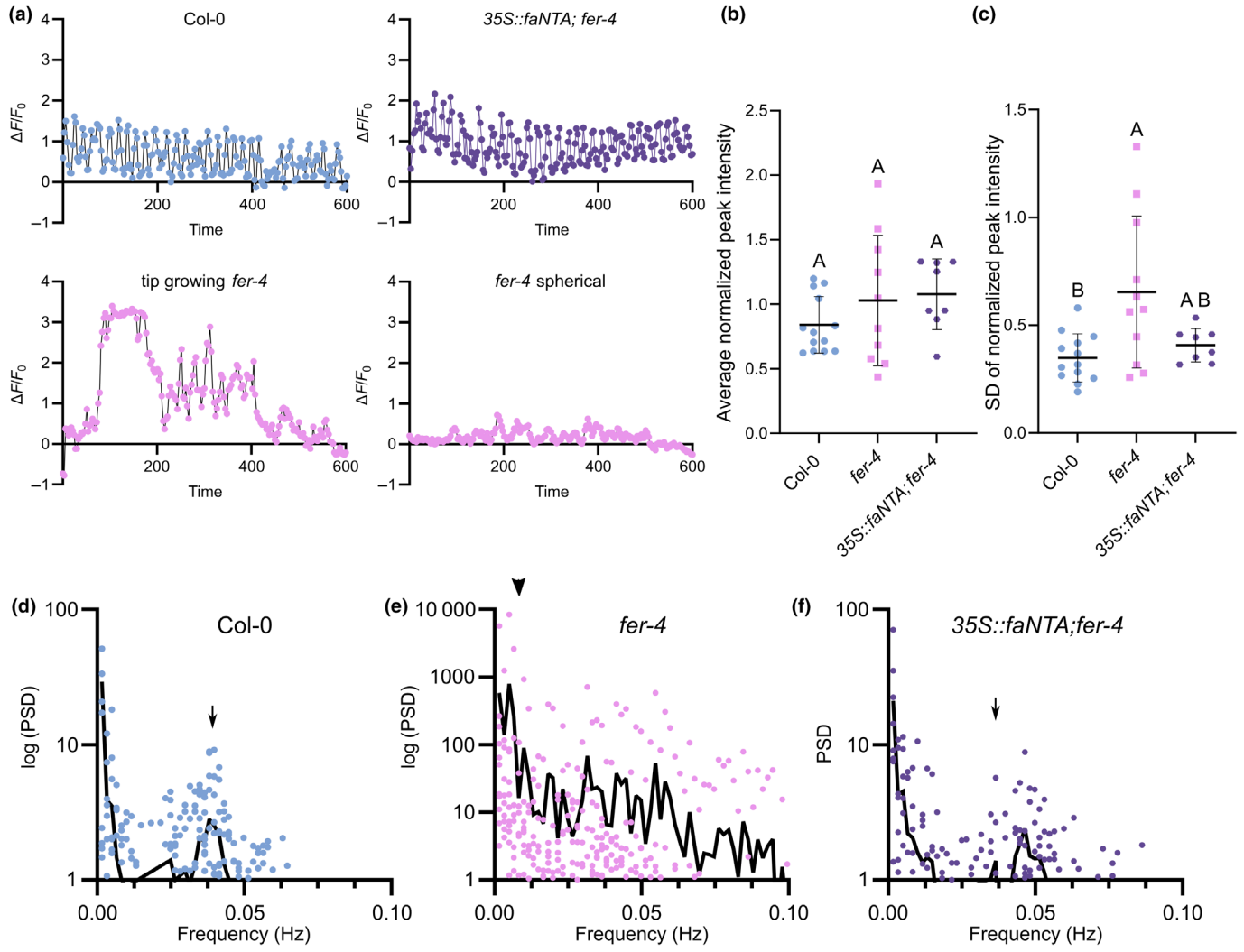

Fig. 2 Arabidopsis *fer-4* root hairs have Ca^{2+} oscillations of erratic amplitude and altered frequency. (a) Normalized R-GECO1 intensity traces for Col-0, *35S::faNTA;fer-4*, tip-growing *fer-4*, and spherical *fer-4* root hairs. Additional traces can be found in Supporting Information Fig. S3. (b, c) Normalized intensity at each peak was extracted for individual root hairs and the average intensity (b) or SD from the average intensity (c) plotted for Col-0 (n = 12), *fer-4* (n = 11), and *35S::faNTA;fer-4* (n = 8). Multiple comparisons were done in GraphPad Prism 10 as a one-way ANOVA with a Tukey test, $P < 0.05$. (d–f) Fourier transform and power spectral density (PSD) analysis results of R-GECO1 normalized signal traces (dots) and mean frequencies (black line) for Col-0, n = 12 (d); tip-growing *fer-4*, n = 11 (e); and *35S::faNTA;fer-4*, n = 8 (f). Arrows indicate the major high frequency peak for Col-0 and *35S::faNTA;fer-4*, and the arrowhead indicates the major low frequency peak for *fer-4*.

reported for Col-0 root hairs expressing R-GECO1 with confocal and RootChip imaging (Candeo *et al.*, 2017; Brost *et al.*, 2019). *fer-4* root hairs have a main low frequency peak at 0.0049 Hz, which corresponds to an oscillation every 204 s (Fig. 2e). *fer-4* root hairs do not have a single high frequency peak; instead, peaks occur with periods of 17–625 s (0.0016–0.059 Hz) (Fig. 2e). The variability in frequency of Ca^{2+} oscillations suggests that one function of FER is to regulate Ca^{2+} influx in root hairs so that oscillations occur at regular intervals. *35S::faNTA; fer-4* root hairs have a single peak at 0.046 Hz and oscillate every 21.7 s, which is a faster oscillatory pattern than Col-0 (26.3 s) (Fig. 2f). These results demonstrate that the lack of a functional FER affects Ca^{2+} oscillations during root hair elongation. faNTA-mediated Ca^{2+} influx is able to complement both the altered amplitude and oscillation patterns in *fer-4* root hairs, which are sufficient to restore normal tip growth to *fer* root hairs.

MLO15 contributes to root hair tip growth

The ability of faNTA to complement *fer* root hair tip growth phenotypes suggests that MLOs may be an important downstream component of FER signaling in growing root hairs. Since faNTA is a chimeric protein and NTA is not expressed in root hairs, we utilized single-cell root transcriptomics data to identify candidate MLO genes expressed during root hair development (Ryu *et al.*, 2019). MLO15 was the most highly expressed MLO in growing root hairs (Fig. S4a). Consistent with the single-cell RNA-seq data, plants expressing *pMLO15::MLO15-GFP* had

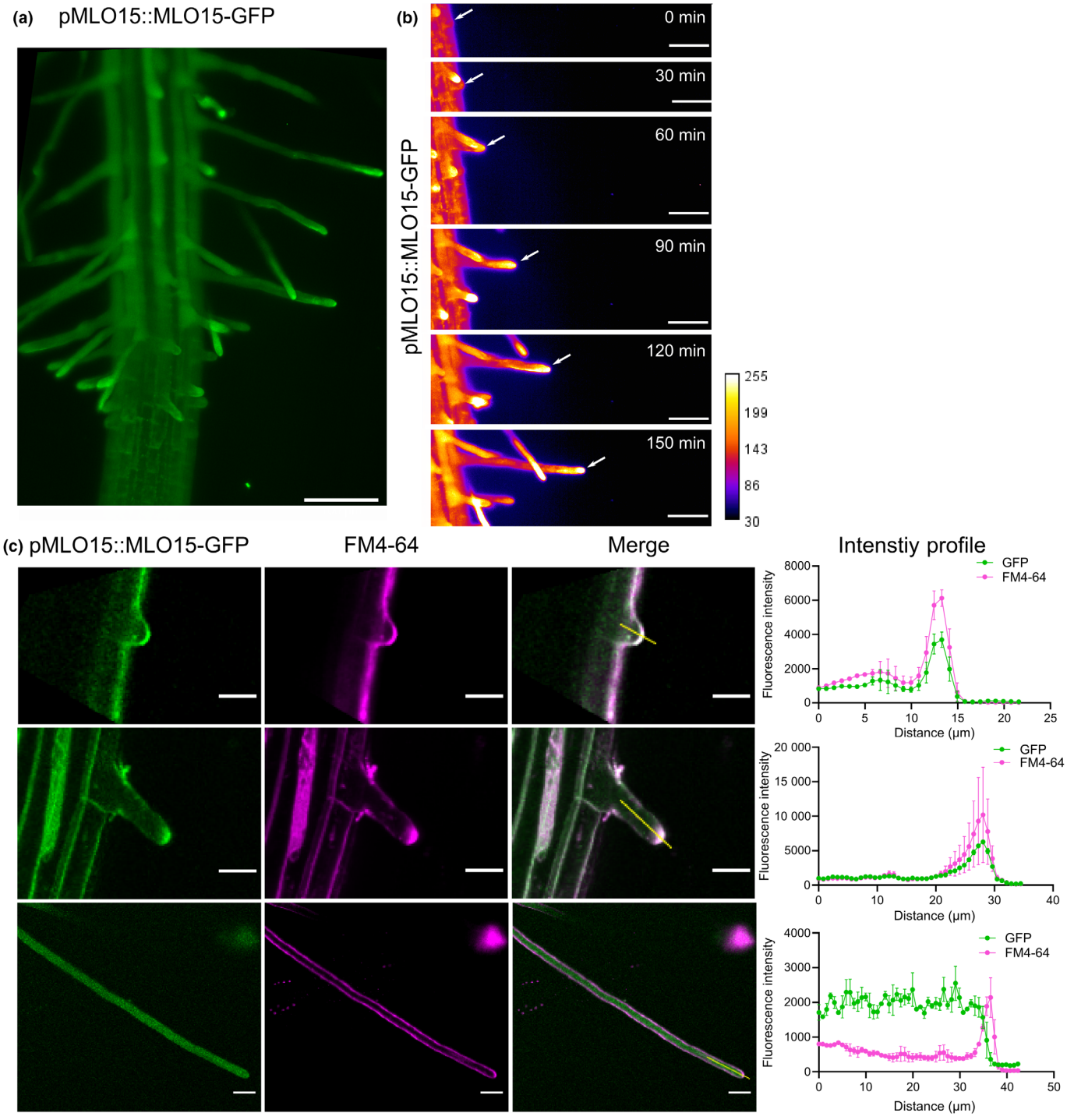

Fig. 3 MLO15 is expressed in Arabidopsis root hairs, and its subcellular localization changes during root hair development. (a) pMLO15::MLO15-GFP signal is expressed higher in root hair epidermal cells than in nonhair epidermal cells. Bar, 100 μm. (b) Light sheet microscopy was used to image MLO15-GFP during root hair initiation and elongation. During root hair initiation, MLO15-GFP signal is weak (0 min), and after rapid elongation begins, MLO15-GFP accumulates at the root apex. Images were pseudocolored to show MLO15-GFP intensity, with white indicating the highest fluorescence. Bars, 50 μm. (c) LCSM was used to image MLO15-GFP in early, elongating, and mature root hairs. FM4-64 staining was used to distinguish the plasma membrane and the root apex. In the root hair bulge, MLO15-GFP accumulates at the plasma membrane. During elongation, MLO15-GFP signal is visible at the plasma membrane and also at the root apex. Mature root hairs show MLO15-GFP signal diffuse throughout the root hair. Intensity profiles of GFP and FM4-64 signal along a line through the root hair (shown in merged images). GFP and FM4-64 signals co-localize at the plasma membrane in root hair bulges and at the plasma membrane and root hair apex in elongating root hairs, but do not co-localize at the plasma membrane in mature root hairs. Bars, 20 μm.

higher GFP signal in root hairs than in nonhair epidermal cells (Fig. 3a).

To determine the root hair growth stages where MLO15 is expressed, LSFM was used to image *pMLO15::MLO15-GFP* roots every 5 min for 4 h. This analysis revealed that the MLO15-GFP signal is low and uniform in initiating root hairs and accumulates at the root tip during active root hair elongation (Fig. 3b, Video S4). Confocal microscopy was used to determine

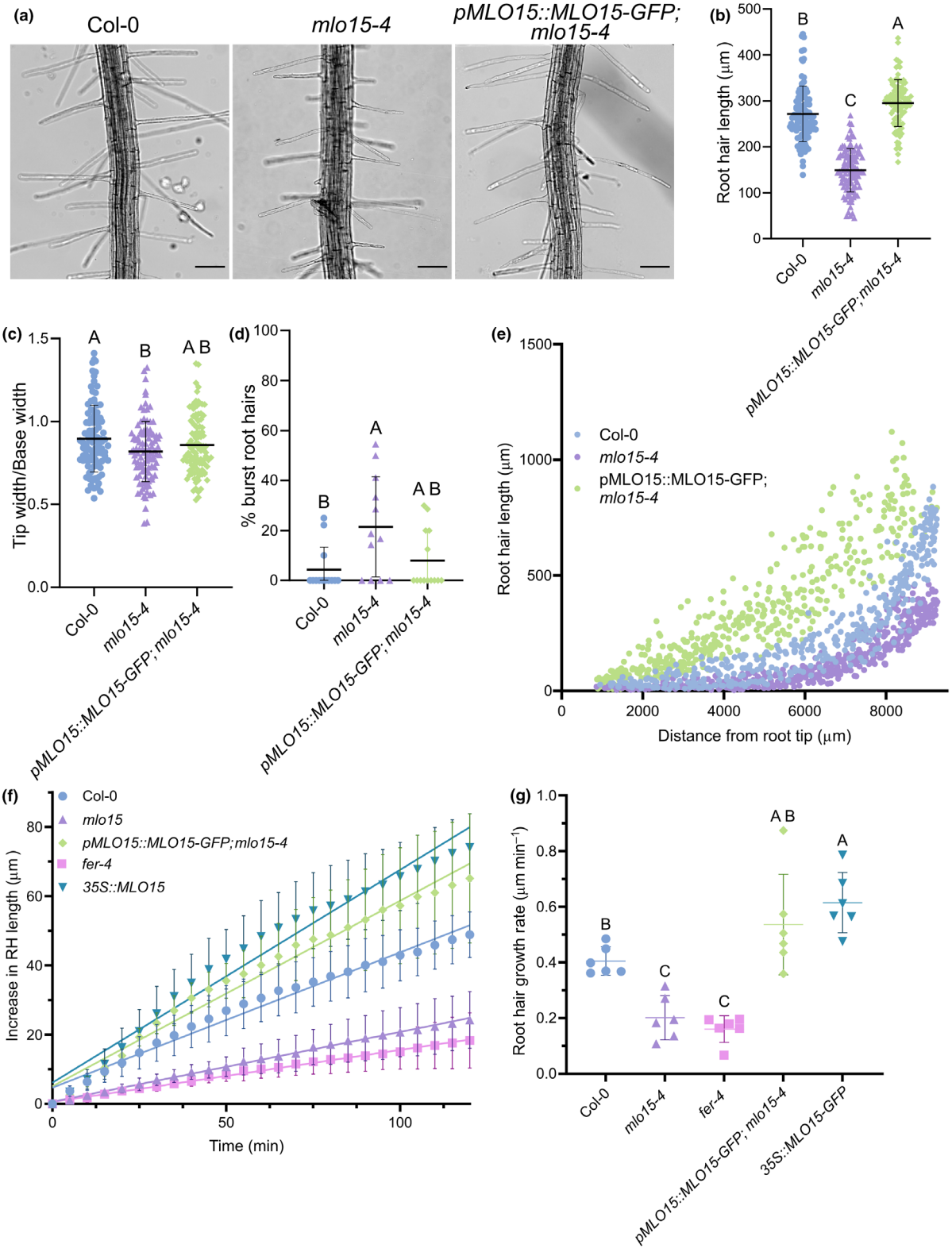

Fig. 4 MLO15 contributes to Arabidopsis root hair elongation. (a–d) Col-0, *mlo15-4*, and *pMLO15::MLO15-GFP;mlo15-4* root hairs were imaged and phenotyped in a 1-mm region located 2–3 mm from the primary root tip (a). Root hair length, tip width/base width, and bursting were quantified for Col-0 (n = 13 seedlings or 100 root hairs), *mlo15-4* (n = 12 seedlings or 98 root hairs), and *pMLO15::MLO15-GFP;mlo15-4* (n = 13 seedlings or 101 root hairs) (b–d). In (b, c), each data point represents a single root hair, while in (d), each data point represents the average of a single root. In the early root hair development region analyzed, *mlo15-4* root hairs are shorter (b), have a slightly lower tip width to base width ratio (c), and have a larger percentage of burst root hairs (d) than Col-0, that is complemented with pMLO15::MLO15-GFP. (e) *mlo15-4* root hairs (n = 465) along the entire primary root have reduced length compared to Col-0 (n = 405) and *pMLO15::MLO15-GFP;mlo15-4* (n = 453). Each data point represents a single root hair. (f, g) MLO15 regulates root hair growth rate. Root hair length was measured every 5 min for 2 h for individual root hairs Col-0 (n = 6), *fer-4* (n = 6), *mlo15-4* (n = 6), *pMLO15::MLO15-GFP;mlo15-4* (n = 5), and *35S::MLO15* (n = 6). Averages are shown in (f) with SE. Root hair growth rate was calculated for individual root hairs by calculating the slope of the regression lines in (f). *mlo15-4* and *fer-4* root hairs elongate at half the rate of the wild-type (g). Bars, 100 μm. Linear regression and statistical comparisons were done in GraphPad Prism 10 with a one-way ANOVA with a Tukey test, $P < 0.05$. Different letters indicate a significant difference and horizontal lines in plots indicate mean ± SD.

the subcellular localization of MLO15-GFP at different stages of root hair development. In early elongating root hairs, MLO15-GFP is present at the plasma membrane of the root hair bulge (Fig. 3c). When root hairs are actively elongating, MLO15-GFP localizes at the plasma membrane along the entire root hair, but also co-localizes with FM4-64 at the root tip (Fig. 3c). FM4-64 labels the root hair apical zone vesicles along with the plasma membrane (Ovecka *et al.*, 2005). In mature root hairs that have stopped growing, MLO15-GFP signal is found in punctate compartments evenly distributed throughout the cytosol and does not appear plasma membrane localized (Fig. 3c). The co-localization of MLO15-GFP and FM4-64 in growing root hairs observed with LSCM is consistent with the LSFM data. MLO15 accumulates at the root hair tip and plasma membrane during elongation and is internalized in mature root hairs, suggesting that MLO15 is involved in root hair growth but is not necessary for the maintenance of mature root hairs.

Since root hairs are tip-growing cells, we hypothesized that MLO15 could be necessary for maintaining tip integrity or tip growth, as these are both processes regulated by FER signaling. If this is true, then we expected that *mlo15* mutants would have similar root hair phenotypes to *fer* mutants. RT-PCR was done on Col-0 and *mlo15-4* root samples to confirm that *mlo15-4* is a knockout allele (Fig. S4b; Methods S1). The length of early elongating root hairs was measured for Col-0, *mlo15-4*, and the complemented line *pMLO15::MLO15-GFP;mlo15-4*. Compared to Col-0, which had an average root hair length of 272 ± 61 μm, *mlo15-4* had shorter root hairs that had an average length of 149 ± 47 μm (Fig. 4a,b). The decreased root hair length of *mlo15-4* was restored to wild-type levels by expressing *pMLO15::MLO15-GFP*, and the complemented line had an average length of 295 ± 50 μm (Fig. 4a,b). To better characterize the reduced root hair length of *mlo15-4*, primary roots of 5-d-old Col-0, *mlo15-4*, and the complemented line *pMLO15::MLO15-GFP; mlo15-4* were imaged, and hairs along the entirety of the primary root were measured. When root hair length was plotted according to the position of that root hair on the primary root, all three genotypes had root hairs that increased in length as they matured. However, in *mlo15-4*, the root hairs only reach half the length of Col-0 root hairs, with a maximum length of *c.* 400 μm compared to 800 μm for Col-0 and 900 μm for the complemented line (Fig. 4e). In *fer-4* mutants, 33.33% of root hairs burst (Fig. 1c). The *mlo15-4* mutant has, on average, 21% root hair bursting compared to the 4% root hair bursting in Col-0 and 8% in the complemented *mlo15-4* line (Fig. 4d). The *mlo15-4* root hair bursting phenotype is not consistent among seedlings imaged, suggesting that some *mlo15-4* roots may be more sensitive to osmotic changes caused from transfer from solid plates to water on slides. We also examined root hair shape in the *mlo15* mutant to see if they are similar to the cone-shaped *fer-4* root hairs. *mlo15-4* root hairs have a slight decrease in the tip width/base width ratio compared to the wild-type. This phenotype is complemented with *pMLO15::MLO15-GFP* (Fig. 4c). Overall, the differences in root hair architecture and shape observed in *mlo15-4* are similar but more subtle than the ones observed for *fer-4* (Fig. 1).

Since the *mlo15-4* mutant had significantly shorter mature root hairs than wild-type roots, we hypothesized that the *mlo15-4* root hairs grow more slowly than wild-type root hairs. Root hair growth over time was measured for Col-0, *fer-4, mlo15-4*, *35S::MLO15*, and *pMLO15::MLO15-GFP;mlo15-4* (Fig. 4f). Consistent with our hypothesis, over the 2-h period, wild-type Col-0 root hairs elongated at a rate of 0.41 ± 0.05 μm min^{-1}, whereas *fer-4* root hairs elongated at 0.16 ± 0.05 μm min^{-1} (half of the root hairs burst during the imaging period and were not measured). The *mlo15-4* mutants had a growth rate comparable to *fer-4* at 0.20 ± 0.08 μm min^{-1}, but did not exhibit the high rate of root hair bursting seen in *fer-4* (Fig. 4g). The complemented *mlo15-4* line and *35S::MLO15* lines elongated even faster than the wild-type at rates of 0.54 ± 0.18 μm min^{-1} and 0.61 ± 0.11 μm min^{-1}, respectively (Fig. 4g).

The root hair growth rates in all genotypes tested were not linear over the entirety of the imaging period, with the first hour having a faster growth rate than the second hour (Fig. 4f). This might be attributed to the seedling's response to altered environmental conditions during imaging and being imaged horizontally, not vertically. To check that expressing R-GECO1 does not affect the root hair phenotypes observed for our lines and to confirm these phenotypes are maintained when roots are grown in the FEP tube system, we calculated root hair growth rates over 10 min for Col-0, *fer-4*, *35S::faNTA; fer-4*, *mlo15-4*, and *35S::MLO15* lines expressing R-GECO1 imaged with LSFM. While all lines had faster root hair growth rates when grown in FEP tubes and imaged vertically, the trends remained the same, with both *mlo15-4* and *fer-4* root hairs having a reduced growth rate compared to Col-0 (Fig. S2h).

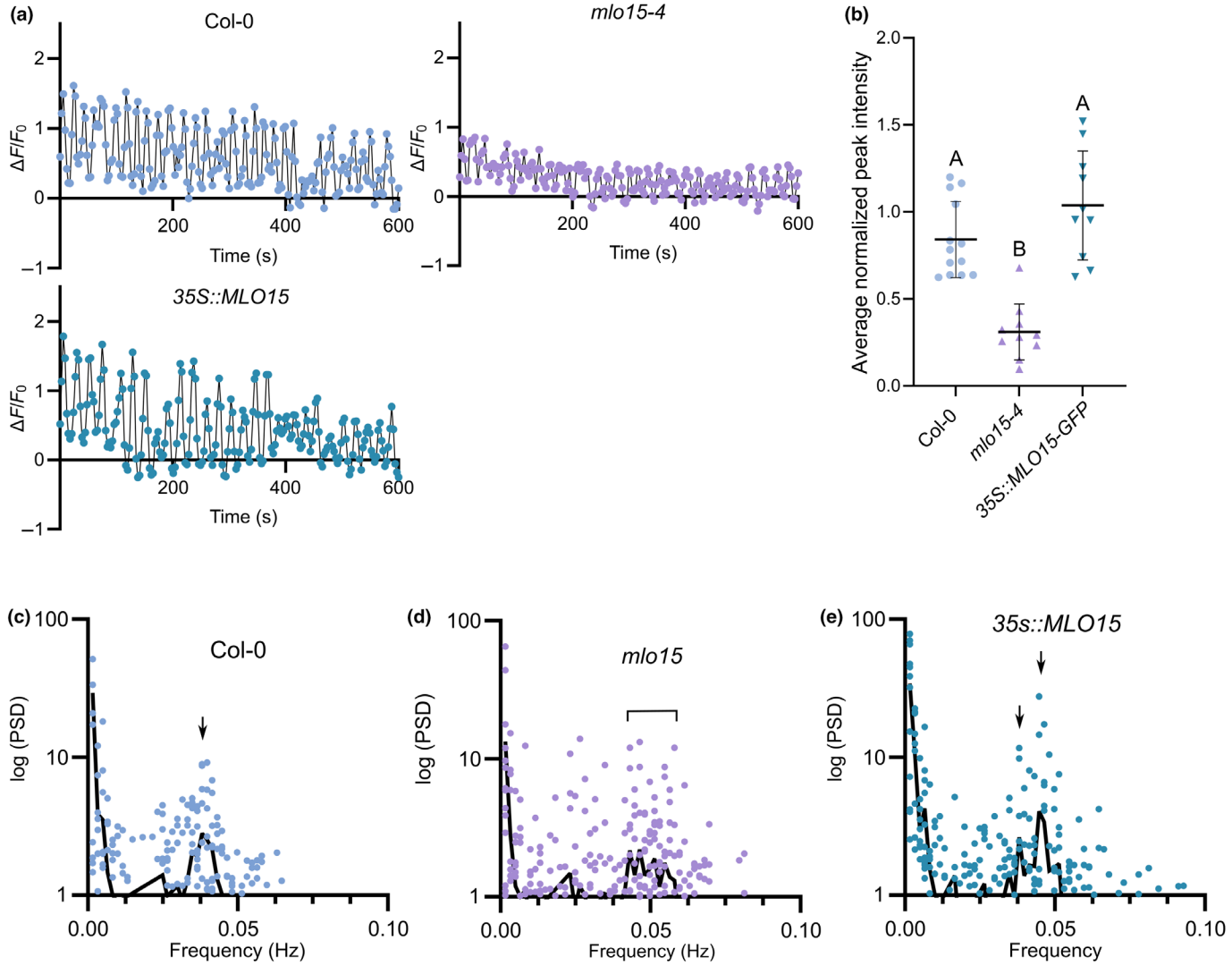

Fig. 5 Arabidopsis *mlo15-4* root hairs have Ca^{2+} oscillations of reduced amplitude and altered frequency. (a) Representative normalized R-GECO1 intensity traces for Col-0, *mlo15-4*, and *35S::MLO15-GFP* root hairs imaged every 3 s for 10 min. Additional traces can be found in Supporting Information Fig. S4. (b) Normalized peak intensity was extracted for individual root hairs, and averages were plotted for Col-0 (n = 12), *mlo15-4* (n = 10), and *35S::MLO15-GFP* (n = 10). Multiple comparisons were done with a one-way ANOVA with Tukey test in GraphPad Prism 10, $P < 0.05$. Different letters indicate a significant difference, and horizontal lines in plots indicate mean ± SD. (c–e) Fourier transformation results of R-GECO1 normalized signal traces (dots) and mean frequencies (black line) for Col-0, n = 12 (c); *mlo15-4*, n = 17 (d), and *35S::MLO15-GFP*, n = 12 (e). Arrows indicate main high frequency peaks for Col-0 and *35S::MLO15*, and brackets indicate high frequency range for *mlo15-4*. The Col-0 data shown in panels (a–c) are duplicated from the data shown in Fig. 2 for easier comparison.

MLO15 regulates Ca^{2+} during root hair growth

Since *mlo15-4* mutants have a similar root hair growth phenotype to *fer-4*, we hypothesized that the reduced root hair elongation rate in *mlo15-4* would also be correlated with reduced $[Ca^{2+}]_{cyt}$ levels. In HEK293 cells, MLO15 was shown to be capable of conducting Ca^{2+} when co-expressed with upstream signaling components (Gao *et al.*, 2023). However, MLO15 has not been shown to regulate $[Ca^{2+}]_{cyt}$ levels in plant cells. To test whether the abnormal root hair development of *mlo15-4* is due to reduced $[Ca^{2+}]_{cyt}$, the Ca^{2+} sensor R-GECO1 in Col-0 was crossed into *mlo15-4* and *35S::MLO15-GFP*. Exogenous ATP treatment confirmed that all lines expressed R-GECO1 at similar levels (Fig. S2e–g). LSFM was used to observe R-GECO1 intensity in early elongating root hairs. Normalized intensity traces show that *mlo15-4* $[Ca^{2+}]_{cyt}$ oscillations occur at a reduced amplitude compared to Col-0, while *35S::MLO15-GFP* oscillations are similar to Col-0 (Fig. 5a; additional traces S5; Videos S2, S5 and S6). Normalized peak intensity was extracted for individual root hairs, and the average peak intensity was compared (Fig. 5b). Compared to Col-0, *mlo15-4* has a significantly reduced average peak intensity, while *35S::MLO15-GFP* has a similar average peak intensity (Fig. 5b).

Altered Ca^{2+} oscillation frequency in root hairs was observed in *fer-4* (Fig. 2) and reported in two double mutants of CNGC-type Ca^{2+} channels, *cngc6;14* and *cngc9;14* (Brost *et al.*, 2019). As previously described in Fig. 2d, Col-0 root hairs had a single peak at 0.038 Hz, which corresponds to oscillations occurring every 26.3 s. *mlo15-4* root hairs have irregular oscillations and an extended peak from 0.04–0.06 Hz that suggests these root hairs oscillate more frequently than Col-0, with oscillations every 17–25 s (Fig. 5d). *fer-4* root hairs also had disrupted oscillation patterning, with a large low frequency peak at 0.0049 Hz and an extended peak from 0.0016 to 0.059 Hz (Fig. 2e). Compared to *fer-4* oscillations, *mlo15-4* oscillations do not show a low frequency peak, and the PSD distribution is less varied. *35S::MLO15-GFP* root hairs have two high frequency peaks: one at 0.038 Hz, which corresponds to a period of 26 s and is the same as Col-0, and one at 0.044 Hz, which corresponds to a 23-s oscillation (Fig. 5e). Together, these data support a function for MLO15 as a regulator of Ca^{2+} influx in root hairs that contributes to normal $[Ca^{2+}]_{cyt}$ oscillations required for root hair growth.

MLO-signaling promotes ROS production in root hairs

The loss of tip integrity in *fer-4* root hairs has previously been attributed to a reduction in ROS (Duan *et al.*, 2010). ROS signaling has been proposed to regulate Ca^{2+} channels, and Ca^{2+} has also been linked to the regulation of RBOH activity (Véry & Davies, 2000; Takeda *et al.*, 2008; Zhang *et al.*, 2018). We have shown that faNTA can bypass FER signaling in root hairs to restore normal $[Ca^{2+}]_{cyt}$ levels to *fer-4*. The next question is whether faNTA can also restore ROS levels in a FER-independent manner.

To determine whether faNTA complementation of *fer-4* also complements the reduction in root hair ROS levels, the nonspecific cell-permeable ROS detector H2DCF-DA that had previously been used to characterize *fer* mutants was used (Duan *et al.*, 2010; Kim *et al.*, 2021). ROS levels in Col-0, *fer-4*, and *35S::faNTA;fer-4* root hairs were quantified (Fig. 6a,b). *fer-4* root hairs had a third of the H2DCF-DA signal as Col-0, whereas *35S::faNTA;fer-4* was not significantly different (Fig. 6b), demonstrating that faNTA is sufficient to increase ROS levels in *fer-4* root hairs. Peroxy Orange 1 (PO1), a cell-permeable dye specific for H_2O_2, was also used to stain root hairs (Fig. 6c,d). Consistent with the H2DCF-DA staining, *fer-4* had a quarter of the PO1 fluorescence compared to Col-0 and *35S::faNTA;fer-4* (Fig. 6d). This staining was repeated on the *fer-1* allele in the Ler background, and faNTA was sufficient to restore ROS levels in *fer-1* with both H2DCF-DA and PO1 staining (Fig. S6a–d). These data suggest that faNTA promotes ROS production in root hairs independently of FER signaling.

Since FER had been shown to be a positive regulator of ROS production through activation of RBOHC (Duan *et al.*, 2010), we hypothesized that faNTA could either act directly or indirectly on RBOHC to bypass FER signaling in root hairs. We tested this hypothesis by introducing *35S::faNTA-YFP* into the *-rhd2-1* allele of the *rbohc* mutant. Imaging confirmed faNTA-YFP expression in root hairs of six independent T1 transformants (Fig. S6e). Compared to Col-0, *rhd2-1* seedlings have shorter root hairs that burst and look similar to *fer-4* (Fig. 6e). faNTA is not able to complement the root hair phenotypes of *rhd2-1* (Fig. 6f). These data suggest that one function of MLO-mediated Ca^{2+} influx is to promote ROS production through activation of RBOHC. We next wanted to determine if there were any differences in ROS accumulation in our *mlo15-4* line that has impaired $[Ca^{2+}]_{cyt}$ oscillations. We predicted that if MLO15 positively regulates ROS levels, then *mlo15-4* root hairs would have reduced ROS, and the *35S::MLO15-GFP* root hairs might have increased ROS. Compared to Col-0, *mlo15-4* has a slight, but significant reduction in PO1 signal compared to Col-0, and the complemented line, and *35S::MLO15-GFP* root hairs have increased signal, indicating that MLO15 may positively regulate ROS production in growing root hairs (Fig. S6g).

Discussion

FER and MLO15 contribute to the regulation of $[Ca^{2+}]_{cyt}$ oscillation amplitude and timing in root hairs

Root hair tip growth involves coordinated Ca^{2+} and ROS signaling to promote growth while maintaining tip integrity. Our study identified new roles for FER and MLO15 in regulating $[Ca^{2+}]_{cyt}$ oscillations during root hair elongation. Both *fer-4* and *mlo15-4* root hairs have oscillations with altered amplitude and disrupted frequency. *mlo15-4* root hairs had a slight increase in root hair bursting compared to the wild-type, but did not have altered root hair initiation. This is consistent with our observation that MLO15 is not highly expressed during root hair initiation, accumulates at the root hair apex and plasma membrane during elongation, and is internalized at root hair maturity. The only other plasma membrane-localized Ca^{2+} channels that have been reported to regulate root hair development are CNGC5, CNGC6, CNGC9, and CNGC14. Single and multiple mutants in the root hair CNGCs have similar phenotypes to *mlo15-4*. The shorter root hair length of *mlo15-4* is similar to the phenotype previously reported for the triple mutant *cngc6,9,14*, and is consistent with pharmacological studies that suggest Ca^{2+} influx is not necessary for the formation of root hair bulges that are the first morphological signs of root hair formation (Schiefelbein *et al.*, 1992; Brost *et al.*, 2019).

In root hairs, $[Ca^{2+}]_{cyt}$ and growth rate oscillations are correlated, with $[Ca^{2+}]_{cyt}$ peaks lagging growth peaks by 5–7 s (Monshausen *et al.*, 2008; Candeo *et al.*, 2017). However, the relevance of the frequency of $[Ca^{2+}]_{cyt}$ oscillations in regulating root hair tip growth rates remains largely unknown. Analyses of calcium dynamics in *mlo15-4* and *cngc* mutants suggest that there is not a linear relationship between oscillation frequency and growth rate. The frequency of $[Ca^{2+}]_{cyt}$ oscillations is shifted slightly lower in *cngc9*, whereas *cngc6,14* and *cngc9,14* root hairs have a loss of normal oscillations, similar to our observations in *fer-4*. The reduced amplitude and faster $[Ca^{2+}]_{cyt}$ oscillations of *mlo15-4* are similar to those of the *cngc14* phenotype, where root hairs have faster oscillations that occur at roughly half the amplitude of Col-0 and have a slower

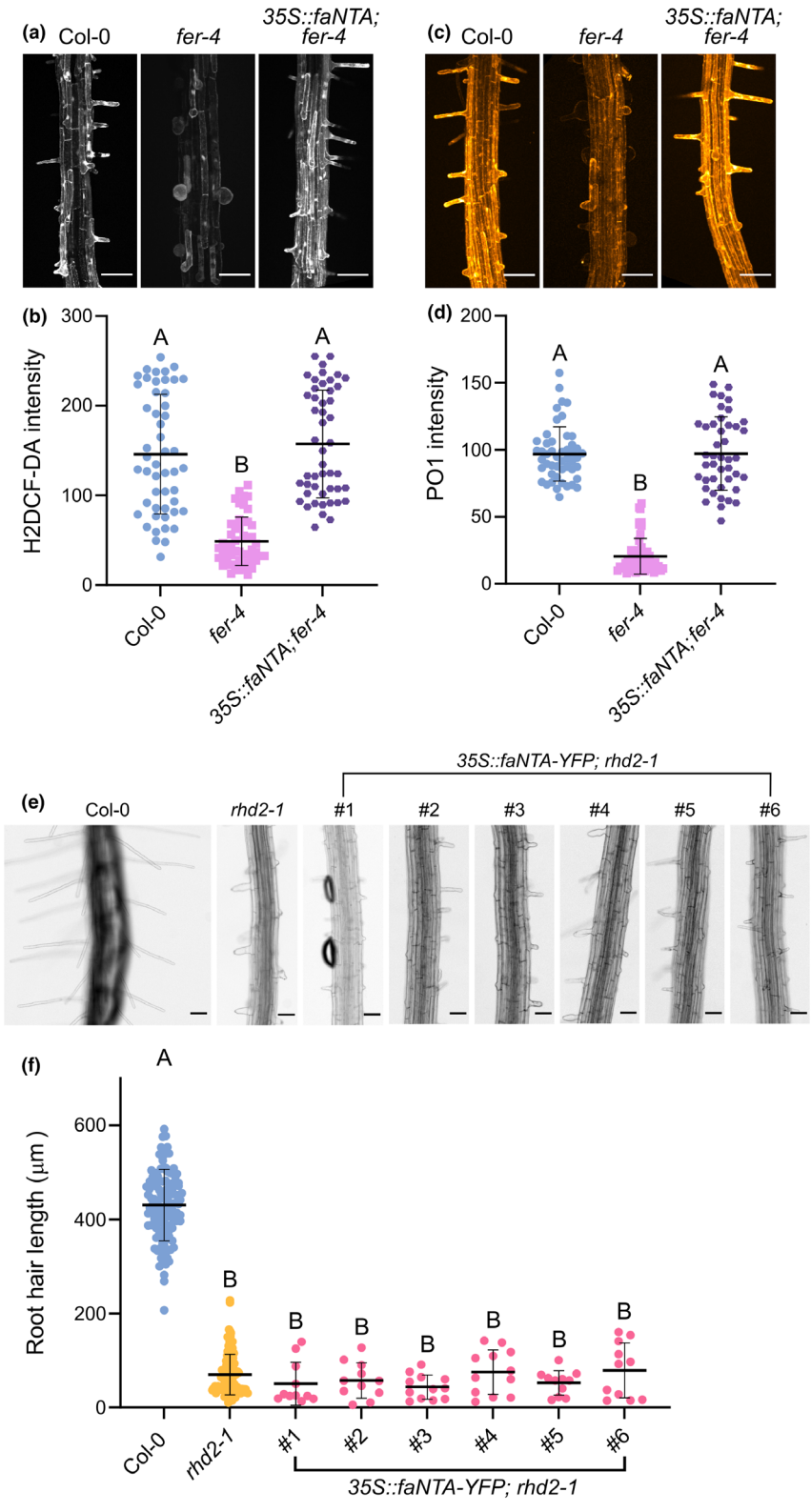

Fig. 6 faNTA complements Arabidopsis *fer-4* ROS, but cannot complement *rhd2-1* root hair defects. (a, b) The general ROS indicator H2DCF-DA was used to compare ROS levels in Col-0 (n = 50), *fer-4* (n = 48), and *35S::faNTA;fer-4* (n = 48) root hairs. (c, d) PO1 staining was used to quantify H_2O_2 levels in Col-0 (n = 49), *fer-4* (n = 54), and *35S::faNTA;fer-4* (n = 43) root hairs. (e, f) Col-0, *rhd2-1*, and *35S::faNTA-YFP; rhd2-1* plants were imaged in a 1-mm region located 2–3 mm from the primary root tip. Root hair length was quantified for Col-0 (n = 10 seedlings), *rhd2-1* (n = 10 seedlings), and six *35S::faNTA-YFP; rhd2-1* T1 plants. Fluorescence intensity and root hair length were compared in GraphPad Prism 10 with a one-way ANOVA with Tukey test, $P < 0.05$. Different letters indicate a significant difference, and horizontal lines in plots indicate mean ± SD. Bars: (a, c) 100 µm; (e) 20 µm.

growth rate (Zhang *et al.*, 2017; Brost *et al.*, 2019). One hypothesis for the reduced growth rate in *mlo15-4* and *cngc14* root hairs despite having more frequent $[Ca^{2+}]_{cyt}$ oscillations is that $[Ca^{2+}]_{cyt}$ needs to reach a certain threshold to activate downstream pathways and that threshold is not achieved as frequently in *mlo15-4* and *cngc14* root hairs. Further work can be done to dissect how $[Ca^{2+}]_{cyt}$ oscillation frequency and amplitude contribute to tip integrity and growth.

Previous studies have shown protein–protein interactions between other members of the MLO and CNGC families (Chen *et al.*, 2012; Meng *et al.*, 2020). Since the phenotypes of *mlo15* and the root hair expressed CNGC mutants are similar, it is possible that MLO15 interacts with CNGCs in root hairs to regulate the amplitude and timing of $[Ca^{2+}]_{cyt}$ oscillations. Both CNGC and MLO channel activity are thought to be regulated by CALMODULIN (CaM) binding at the C-terminus (Fischer *et al.*, 2013, 2017; Gao *et al.*, 2022; Yuan *et al.*, 2025). Whether CaM binding functions to negatively regulate Ca^{2+} influx and maintain $[Ca^{2+}]_{cyt}$ oscillations in root hairs needs further investigation.

$[Ca^{2+}]_{cyt}$ and ROS crosstalk during root hair development

$[Ca^{2+}]_{cyt}$ oscillations and a tip-focused ROS gradient function synergistically to promote tip growth of root hairs (Monshausen *et al.*, 2009). The *rhd2/rbohc* mutant has root hairs with altered tip integrity that burst. *rhd2* root hairs also have lower $[Ca^{2+}]_{cyt}$ levels that can be increased with the addition of ROS (Foreman *et al.*, 2003). The *rhd2* tip integrity phenotype is rescued, and tip-focused $[Ca^{2+}]_{cyt}$ oscillations are restored when the media pH is increased to 6 (Monshausen *et al.*, 2007). This suggests that one function of the ROS generated by RBOHC is to activate Ca^{2+} influx channels, but that RBOHC is not essential for the formation of the $[Ca^{2+}]_{cyt}$ gradient. The abnormal root hair development of *fer-4* was previously attributed to a reduction of ROS (Duan *et al.*, 2010). Our results confirm reduced ROS levels in *fer-4* and also show *fer-4* root hairs have altered $[Ca^{2+}]_{cyt}$ oscillations with lower frequency and reduced amplitude. We have also shown that faNTA is not able to complement the impaired root hair development of *rhd2-1/rbohc*. An outstanding question remains whether FER regulates $[Ca^{2+}]_{cyt}$ oscillations through direct regulation of Ca^{2+} channels or if the reduction in ROS in *fer-4* leads to altered regulation of Ca^{2+} channels and disrupted $[Ca^{2+}]_{cyt}$ oscillations.

Our finding that faNTA was able to complement ROS production in *fer* root hairs suggests that the increased $[Ca^{2+}]_{cyt}$ induces ROS production independently from the well-described FER/ROP-GEF/RBOHC signal transduction pathway described in (Duan *et al.*, 2010). Ca^{2+} signaling can activate RBOHC to produce ROS in root hairs through multiple mechanisms. Ca^{2+}-dependent phosphorylation of RBOHC through CALCINEURIN B-LIKE PROTEIN 1 (CBL1) and CBL-INTERACTING PROTEIN KINASE 26 (CIPK26) can activate RBOHC, but is not required for normal root hair growth (Zhang *et al.*, 2018). Alternatively, RBOHC has two cytosolic EF-hand domains that can bind Ca^{2+}. The EF-hand domains are necessary for RBOHC function in root hairs, and when these EF-hands are mutated to abolish Ca^{2+} binding, RBOHC cannot complement the *rhd2* phenotype (Takeda *et al.*, 2008). It is possible that the restoration of ROS in *fer-4* root hairs occurs through faNTA-mediated Ca^{2+} influx that activates RBOHC through Ca^{2+} binding at the EF-hand motifs. In support of this, a recent study has shown that Ca^{2+} influx regulated by CNGC14 is required for the RBOHC/F-mediated ROS burst in primary roots in response to exogenous auxin treatment (Kulich *et al.*, 2025a,b). More work needs to be done to dissect the mechanism of faNTA complementation of *fer-4* to determine if the complementation of ROS is in fact due to an increase in $[Ca^{2+}]_{cyt}$.

MLOs as amplifiers of FER signaling

We previously showed that faNTA could bypass FER signaling in synergid cells during pollen tube reception, indicating a possible mechanism where MLO channels amplify FER signaling responses (Ju *et al.*, 2021). In this study, we found that faNTA could also complement root hair growth phenotypes in *fer*, suggesting that a similar booster mechanism may be in play. It remains unclear how $[Ca^{2+}]_{cyt}$ oscillations are initiated in root hairs, but we now know that these oscillations are maintained through MLO and CNGC function (Zhang *et al.*, 2017; Tan *et al.*, 2020).

Outside of pollen tube reception and root hair development, MLOs have been implicated in similar signaling processes as FER, including powdery mildew susceptibility and root thigmotropism (Consonni *et al.*, 2006; Chen *et al.*, 2009; Kessler *et al.*, 2010; Bidzinski *et al.*, 2014; Shih *et al.*, 2014; Darwish *et al.*, 2022). In most instances, *fer* plants have a more severe phenotype than the *mlo*, or multiple *mlos* need to be knocked out to display the same phenotype as *fer*. Further work can be done to determine whether there is a conserved role for MLOs functioning downstream of FER as amplifiers of FER signaling throughout the plant.

How is MLO15 regulated?

faNTA is sufficient to restore normal $[Ca^{2+}]_{cyt}$ oscillations and ROS levels to *fer-4* root hairs, but it remains unclear whether FER is required for MLO15 activation in root hairs. Two modes of MLO activation have been described previously. (1) FER activates NTA (MLO7) by regulating its trafficking to the filiform apparatus in synergids and (2) the FER homologs ANX1/2 and BUPS1/2 activate MLO1/5/9/15 in pollen tubes through activating a cytoplasmic kinase intermediate MARIS (MRI) (Ju *et al.*, 2021; Gao *et al.*, 2022, 2023). MLO15 is unable to conduct Ca^{2+} when expressed by itself in HEK293 cells, but can mediate Ca^{2+} influx when co-expressed with upstream signaling genes (Gao *et al.*, 2023). It is possible that MLO15 activation in root hairs is similar to its activation in pollen tubes where FER activates MRI that then activates MLO15. A constitutively active *mri* mutant can complement *fer* root hair phenotypes, but MRI has not been implicated in Ca^{2+} signaling in root hairs, and it remains unknown whether *mri* root hairs have altered $[Ca^{2+}]_{cyt}$ oscillations (Boisson-Dernier *et al.*, 2015; Liao *et al.*, 2016). Alternatively, FER has been shown to form signaling complexes with other CrRLK1L proteins in other cell types (Galindo-Trigo *et al.*, 2020; Liu *et al.*, 2021). CAPS1/ERU is a CrRLK1L protein that is also required for normal $[Ca^{2+}]_{cyt}$ oscillations in root hairs (Kwon *et al.*, 2018). It is possible that MLO15 is a target of

ERU or an ERU/FER complex. A third possibility is that FER regulates MLO15 subcellular localization. MLO15 has different subcellular localization patterns in growing vs mature root hairs, which could be analogous to the FER/NTA system, where NTA is retained in the Golgi until FER signaling is activated by the arriving pollen tubes, upon which it accumulates at the filiform apparatus (Ju *et al.*, 2021). A similar mechanism could be employed in root hairs, where FER signaling is on during active growth and leads to the accumulation of MLO15 at the plasma membrane. When root hairs reach maturity and no longer need to grow, FER signaling would be turned down, inhibiting MLO15 accumulation in the plasma membrane. At this time, we also cannot rule out the possibility that MLO15 is regulated independently of FER in root hairs, and FER instead activates other families of Ca^{2+} channels. Future work should focus on elucidating how FER regulates $[Ca^{2+}]_{cyt}$ oscillations in root hairs and on determining if this is through direct activation of MLO15.

Acknowledgements

We thank Marilyn Vargas and Molly Kosiba for assisting with experiments, the Bindley Bioscience Center Imaging Facility for assistance with confocal microscopy, the Purdue Plant Growth Facility for assistance with plant cultivation, and the Arabidopsis Biological Resource Center for providing seed stocks. We thank the Purdue Office of the Vice President for Research for providing funding for the Bruker light sheet microscope. We also thank Dr Leonor Boavida, Dr Anjali Iyer-Pascuzzi, Dr Tesfaye Mengiste, and Sowmiya Devi Venkatesan for helpful discussions. This work was supported by funding from the National Science Foundation (IOS-2224038) to SAK and a USDA National Institute of Food and Agriculture Pre-Doctoral Fellowship (2023-67011-40330) to STO. WZ and CJS were supported by the EMBRIO Institute, contract #2120200, a National Science Foundation (NSF) Biology Integration Institute.

Competing interests

None declared.

Author contributions

STO, WZ, CJS and SAK conceived and designed the experiments. STO and WZ performed the experiments. STO, WZ and SAK analyzed the data. STO and SAK wrote the manuscript, and all authors revised and approved the final manuscript.

ORCID

Sharon A. Kessler https://orcid.org/0000-0002-7964-0451
Sienna T. Ogawa https://orcid.org/0000-0001-6981-7113
Christopher J. Staiger https://orcid.org/0000-0003-2321-1671
Weiwei Zhang https://orcid.org/0000-0002-4754-6241

Data availability

Sequence data from this article can be found in GenBank/EMBL data libraries under accession numbers AT3G51550 (FER) and AT2G44110 (MLO15). The relevant MATLAB code can be found in link: https://github.com/SADDLab/Root_Hair_Calcium_Analysis_Toolkit.git.

References

Bibikova TN, Zhigilei A, Gilroy S. 1997. Root hair growth in *Arabidopsis thaliana* is directed by calcium and an endogenous polarity. *Planta* **203**: 495–505.

Bidzinski P, Noir S, Shahi S, Reinstädler A, Gratkowska DM, Panstruga R. 2014. Physiological characterization and genetic modifiers of aberrant root thigmomorphogenesis in mutants of *Arabidopsis thaliana* MILDEW LOCUS O genes. *Plant, Cell & Environment* **37**: 2738–2753.

Boisson-Dernier A, Franck CM, Lituiev DS, Grossniklaus U. 2015. Receptor-like cytoplasmic kinase MARIS functions downstream of CrRLK1L-dependent signaling during tip growth. *Proceedings of the National Academy of Sciences, USA* **112**: 12211–12216.

Brost C, Studtrucker T, Reimann R, Denninger P, Czekalla J, Krebs M, Fabry B, Schumacher K, Grossmann G, Dietrich P. 2019. Multiple cyclic nucleotide-gated channels coordinate calcium oscillations and polar growth of root hairs. *The Plant Journal* **99**: 910–923.

Büschges R, Hollricher K, Panstruga R, Simons G, Wolter M, Frijters A, van Daelen R, van der Lee T, Diergaarde P, Groenendijk J *et al.* 1997. The barley Mlo gene: a novel control element of plant pathogen resistance. *Cell* **88**: 695–705.

Candeo A, Doccula FG, Valentini G, Bassi A, Costa A. 2017. Light sheet fluorescence microscopy quantifies calcium oscillations in root hairs of *Arabidopsis thaliana*. *Plant & Cell Physiology* **58**: 1161–1172.

Chen J, Lalonde S, Obrdlik P, Noorani Vatani A, Parsa SA, Vilarino C, Revuelta JL, Frommer WB, Rhee SY. 2012. Uncovering Arabidopsis membrane protein interactome enriched in transporters using mating-based split ubiquitin assays and classification models. *Frontiers in Plant Science* **3**: 124.

Chen Z, Noir S, Kwaaitaal M, Hartmann HA, Wu MJ, Mudgil Y, Sukumar P, Muday G, Panstruga R, Jones AM. 2009. Two seven-transmembrane domain MILDEW RESISTANCE LOCUS O proteins cofunction in Arabidopsis root thigmomorphogenesis. *Plant Cell* **21**: 1972–1991.

Cheung AY. 2024. FERONIA: a receptor kinase at the core of a global signaling network. *Annual Review of Plant Biology* **75**: 345–375.

Clough SJ, Bent AF. 1998. Floral dip: a simplified method for Agrobacterium-mediated transformation of *Arabidopsis thaliana*. *The Plant Journal* **16**: 735–743.

Cole RA, Fowler JE. 2006. Polarized growth: maintaining focus on the tip. *Current Opinion in Plant Biology* **9**: 579–588.

Consonni C, Humphry ME, Hartmann HA, Livaja M, Durner J, Westphal L, Vogel J, Lipka V, Kemmerling B, Schulze-Lefert P *et al.* 2006. Conserved requirement for a plant host cell protein in powdery mildew pathogenesis. *Nature Genetics* **38**: 716–720.

Curtis MD, Grossniklaus U. 2003. A gateway cloning vector set for high-throughput functional analysis of genes *in planta*. *Plant Physiology* **133**: 462–469.

Darwish E, Ghosh R, Ontiveros-Cisneros A, Tran HC, Petersson M, De Milde L, Broda M, Goossens A, Van Moerkercke A, Khan K *et al.* 2022. Touch signaling and thigmomorphogenesis are regulated by complementary CAMTA3- and JA-dependent pathways. *Science Advances* **8**: eabm2091.

Davis TC, Jones DS, Dino AJ, Cejda NI, Yuan J, Willoughby AC, Kessler SA. 2017. *Arabidopsis thaliana* MLO genes are expressed in discrete domains during reproductive development. *Plant Reproduction* **30**: 185–195.

Demidchik V, Nichols C, Oliynyk M, Dark A, Glover BJ, Davies JM. 2003. Is ATP a signaling agent in plants? *Plant Physiology* **133**: 456–461.

Duan Q, Kita D, Li C, Cheung AY, Wu HM. 2010. FERONIA receptor-like kinase regulates RHO GTPase signaling of root hair development. *Proceedings of the National Academy of Sciences, USA* **107**: 17821–17826.

Escobar-Restrepo JM, Huck N, Kessler S, Gagliardini V, Gheyselinck J, Yang WC, Grossniklaus U. 2007. The FERONIA receptor-like kinase mediates male-female interactions during pollen tube reception. *Science* **317**: 656–660.

Fischer C, DeFalco TA, Karia P, Snedden WA, Moeder W, Yoshioka K, Dietrich P. 2017. Calmodulin as a Ca^{2+}-sensing subunit of Arabidopsis cyclic nucleotide-gated channel complexes. *Plant and Cell Physiology* **58**: 1208–1221.

Fischer C, Kugler A, Hoth S, Dietrich P. 2013. An IQ domain mediates the interaction with calmodulin in a plant cyclic nucleotide-gated channel. *Plant & Cell Physiology* **54**: 573–584.

Foreman J, Demidchik V, Bothwell JH, Mylona P, Miedema H, Torres MA, Linstead P, Costa S, Brownlee C, Jones JD *et al.* 2003. Reactive oxygen species produced by NADPH oxidase regulate plant cell growth. *Nature* **422**: 442–446.

Galindo-Trigo S, Blanco-Touriñán N, DeFalco TA, Wells ES, Gray JE, Zipfel C, Smith LM. 2020. CrRLK1L receptor-like kinases HERK1 and ANJEA are female determinants of pollen tube reception. *EMBO Reports* **21**: e48466.

Gao Q, Wang C, Xi Y, Shao Q, Hou C, Li L, Luan S. 2023. RALF signaling pathway activates MLO calcium channels to maintain pollen tube integrity. *Cell Research* **33**: 71–79.

Gao Q, Wang C, Xi Y, Shao Q, Li L, Luan S. 2022. A receptor-channel trio conducts Ca^{2+} signalling for pollen tube reception. *Nature* **607**: 534–539.

Gayomba SR, Muday GK. 2020. Flavonols regulate root hair development by modulating accumulation of reactive oxygen species in the root epidermis. *Development* **147**: 254.

Hoffmann RD, Olsen LI, Ezike CV, Pedersen JT, Manstretta R, López-Marqués RL, Palmgren M. 2019. Roles of plasma membrane proton ATPases AHA2 and AHA7 in normal growth of roots and root hairs in *Arabidopsis thaliana*. *Physiologia Plantarum* **166**: 848–861.

Ju Y, Yuan J, Jones DS, Zhang W, Staiger CJ, Kessler SA. 2021. Polarized NORTIA accumulation in response to pollen tube arrival at synergids promotes fertilization. *Developmental Cell* **56**: 2938–2951.

Keinath NF, Waadt R, Brugman R, Schroeder JI, Grossmann G, Schumacher K, Krebs M. 2015. Live cell imaging with R-GECO1 sheds light on flg22- and chitin-induced transient [Ca(2+)]cyt patterns in Arabidopsis. *Molecular Plant* **8**: 1188–1200.

Kessler SA, Shimosato-Asano H, Keinath NF, Wuest SE, Ingram G, Panstruga R, Grossniklaus U. 2010. Conserved molecular components for pollen tube reception and fungal invasion. *Science* **330**: 968–971.

Kim D, Yang J, Gu F, Park S, Combs J, Adams A, Mayes HB, Jeon SJ, Bahk JD, Nielsen E. 2021. A temperature-sensitive FERONIA mutant allele that alters root hair growth. *Plant Physiology* **185**: 405–423.

Kulich I, Oulehlová D, Vladimirtsev D, Zhou M, Lileikyte E, Janda M, Iakovenko O, Neubergerová M, Studtrucker T, Pleskot R *et al.* 2025a. Armadillo repeat only proteins are crucial for the function of plant CNGC channels. *bioRxiv*. doi: 10.1101/2025.01.06.631460.

Kulich I, Vladimirtsev D, Randuch M, Gao S, Citterico M, Konrad KR, Nagel G, Wrzaczek M, Friml J. 2025b. Calcium-triggered apoplastic ROS bursts balance gravity and mechanical signals to navigate soil. *bioRxiv*. doi: 10.1101/2025.01.07.631646.

Kwon T, Sparks JA, Liao F, Blancaflor EB. 2018. ERULUS is a plasma membrane-localized receptor-like kinase that specifies root hair growth by maintaining tip-focused cytoplasmic calcium oscillations. *Plant Cell* **30**: 1173–1177.

Liao HZ, Zhu MM, Cui HH, Du XY, Tang Y, Chen LQ, Ye D, Zhang XQ. 2016. MARIS plays important roles in Arabidopsis pollen tube and root hair growth. *Journal of Integrative Plant Biology* **58**: 927–940.

Liu C, Shen L, Xiao Y, Vyshedsky D, Peng C, Sun X, Liu Z, Cheng L, Zhang H, Han Z *et al.* 2021. Pollen PCP-B peptides unlock a stigma peptide-receptor kinase gating mechanism for pollination. *Science* **372**: 171–175.

Lopez LE, Ibeas MA, Diaz Dominguez G, Estevez JM. 2024. Exploring the puzzle of reactive oxygen species acting on root hair cells. *Journal of Experimental Botany* **75**: 4589–4598.

Mendrinna A, Persson S. 2015. Root hair growth: it's a one way street. *F1000Prime Reports* **7**: 23.

Meng JG, Liang L, Jia PF, Wang YC, Li HJ, Yang WC. 2020. Integration of ovular signals and exocytosis of a Ca(2+) channel by MLOs in pollen tube guidance. *Nature Plants* **6**: 143–153.

Monshausen GB, Bibikova TN, Messerli MA, Shi C, Gilroy S. 2007. Oscillations in extracellular pH and reactive oxygen species modulate tip growth of Arabidopsis root hairs. *Proceedings of the National Academy of Sciences, USA* **104**: 20996–21001.

Monshausen GB, Bibikova TN, Weisenseel MH, Gilroy S. 2009. Ca^{2+} regulates reactive oxygen species production and pH during mechanosensing in Arabidopsis roots. *Plant Cell* **21**: 2341–2356.

Monshausen GB, Messerli MA, Gilroy S. 2008. Imaging of the Yellow Cameleon 3.6 indicator reveals that elevations in cytosolic Ca^{2+} follow oscillating increases in growth in root hairs of Arabidopsis. *Plant Physiology* **147**: 1690–1698.

Myers ZA, Kumimoto RW, Siriwardana CL, Gayler KK, Risinger JR, Pezzetta D, Holt Iii BF. 2016. NUCLEAR FACTOR Y, Subunit C (NF-YC) transcription factors are positive regulators of photomorphogenesis in *Arabidopsis thaliana*. *PLoS Genetics* **12**: e1006333.

Ngo QA, Vogler H, Lituiev DS, Nestorova A, Grossniklaus U. 2014. A calcium dialog mediated by the FERONIA signal transduction pathway controls plant sperm delivery. *Developmental Cell* **29**: 491–500.

Odell JT, Nagy F, Chua NH. 1985. Identification of DNA sequences required for activity of the cauliflower mosaic virus 35S promoter. *Nature* **313**: 810–812.

Ogawa ST, Kessler SA. 2023. Update on signaling pathways regulating polarized intercellular communication in Arabidopsis reproduction. *Plant Physiology* **193**: 1732–1744.

Ovecka M, Lang I, Baluska F, Ismail A, Illes P, Lichtscheidl IK. 2005. Endocytosis and vesicle trafficking during tip growth of root hairs. *Protoplasma* **226**: 39–54.

Ryu KH, Huang L, Kang HM, Schiefelbein J. 2019. Single-Cell RNA sequencing resolves molecular relationships among individual plant cells. *Plant Physiology* **179**: 1444–1456.

Schiefelbein JW, Shipley A, Rowse P. 1992. Calcium influx at the tip of growing root-hair cells of *Arabidopsis thaliana*. *Planta* **187**: 455–459.

Schindelin J, Arganda-Carreras I, Frise E, Kaynig V, Longair M, Pietzsch T, Preibisch S, Rueden C, Saalfeld S, Schmid B *et al.* 2012. Fiji: an open-source platform for biological-image analysis. *Nature Methods* **9**: 676–682.

Shih HW, Miller ND, Dai C, Spalding EP, Monshausen GB. 2014. The receptor-like kinase FERONIA is required for mechanical signal transduction in Arabidopsis seedlings. *Current Biology* **24**: 1887–1892.

Stéger A, Palmgren M. 2022. Root hair growth from the pH point of view. *Frontiers in Plant Science* **13**: 949672.

Takatsuka H, Ito M. 2020. Cytoskeletal control of planar polarity in root hair development. *Frontiers in Plant Science* **11**: 580935.

Takeda S, Gapper C, Kaya H, Bell E, Kuchitsu K, Dolan L. 2008. Local positive feedback regulation determines cell shape in root hair cells. *Science* **319**: 1241–1244.

Tan YQ, Yang Y, Zhang A, Fei CF, Gu LL, Sun SJ, Xu W, Wang L, Liu H, Wang YF. 2020. Three CNGC family members, CNGC5, CNGC6, and CNGC9, are required for constitutive growth of Arabidopsis root hairs as Ca^{2+}-permeable channels. *Plant Communications* **1**: 100001.

Tinevez JY, Perry N, Schindelin J, Hoopes GM, Reynolds GD, Laplantine E, Bednarek SY, Shorte SL, Eliceiri KW. 2017. TrackMate: an open and extensible platform for single-particle tracking. *Methods* **115**: 80–90.

Véry AA, Davies JM. 2000. Hyperpolarization-activated calcium channels at the tip of Arabidopsis root hairs. *Proceedings of the National Academy of Sciences, USA* **97**: 9801–9806.

Weber M, Mickoleit M, Huisken J. 2014. Multilayer mounting for long-term light sheet microscopy of zebrafish. *Journal of Visualized Experiments* **2**: 3541.

Yuan J, Ogawa ST, Jones DS, Lucca N, Ju Y, Kessler SA. 2025. Regulation of MLO trafficking by calmodulin binding domains. *Journal of Experimental Botany* **2**: 52–69.

Zhang S, Pan Y, Tian W, Dong M, Zhu H, Luan S, Li L. 2017. Arabidopsis CNGC14 mediates calcium influx required for tip growth in root hairs. *Molecular Plant* **10**: 1004–1006.

Zhang X, Köster P, Schlücking K, Balcerowicz D, Hashimoto K, Kuchitsu K, Vissenberg K, Kudla J. 2018. CBL1-CIPK26-mediated phosphorylation enhances activity of the NADPH oxidase RBOHC, but is dispensable for root hair growth. *FEBS Letters* **592**: 2582–2593.

Zhu M, Du BY, Tan YQ, Yang Y, Zhang Y, Wang YF. 2025. CPK1 activates CNGCs through phosphorylation for Ca^{2+} signaling to promote root hair growth in Arabidopsis. *Nature Communications* **16**: 676.

Supporting Information

Additional Supporting Information may be found online in the Supporting Information section at the end of the article.

Fig. S1 faNTA is plasma membrane localized and complements the abnormal root hair development of *fer-1*.

Fig. S2 R-GECO1 is expressed similarly in all lines and does not affect root hair phenotypes.

Fig. S3 Additional normalized intensity traces of R-GECO1 intensity over 10 min in Col-0, *fer-4*, and *35S::faNTA;fer-4*.

Fig. S4 Expression of MLOs in root hair and nonhair epidermal cells.

Fig. S5 Additional normalized intensity traces of R-GECO1 intensity over 10 min in Col-0, *mlo15-4*, and *35S::MLO15*.

Fig. S6 MLOs positively regulate ROS production in root hairs.

Methods S1 Methods for ATP treatment of root hair and RT-PCR experiments in S2 and S4.

Video S1 R-GECO1 in Col-0 root hairs.

Video S2 R-GECO1 in *fer-4* root hairs.

Video S3 R-GECO1 in *35S::faNTA-YFP;fer-4* root hairs.

Video S4 MLO15-GFP expression during root hair development.

Video S5 R-GECO1 in *mlo15-4* root hairs.

Video S6 R-GECO1 in *35S::MLO15-GFP* root hairs.

Please note: Wiley is not responsible for the content or functionality of any Supporting Information supplied by the authors. Any queries (other than missing material) should be directed to the *New Phytologist* Central Office.